National Institute of Laser Enhanced Sciences, JLSA's Vol.02. Issue.1 (2025)
DOI: 10.21608/JLSA.2025.377593.1033

NILES

Journal of Laser Science and Applications
journal homepage: https://jlsa.journals.ekb.eg

Cairo University

Review "Exploring 2D Graphene Analogues for Advanced Photodetection Applications"

Ahmed Abdelhady A. Khalil[*a,b], Samar Akef[b], Heba A. Shawkey[c], Mohamed A. Swillam[b]

[a] Laser Sciences and Interactions Department, National Institute of Laser Enhanced Sciences (NILES), Cairo University, Giza 12613, Egypt.
[b] Physics Department, School of Science and Engineering (SSE), The American University in Cairo, Cairo 11835, Egypt.
[c] Microelectronics Department, Electronics Research Institute (ERI), Cairo, Egypt.

Abstract:
Extensive research has been conducted on layered transition metal dichalcogenides (TMDCs) to explore their potential as substitutes for graphene and other emerging two-dimensional layered materials (2DLMs). TMDCs constitute a versatile family of 2D materials exhibiting exceptional optical properties, positioning them as highly promising candidates for the development of advanced, multifunctional, high-performance optoelectronic devices. The tunability of their band gap energies - particularly in molybdenum and tungsten disulfides - enables precise control over their electronic properties, facilitating their transition from insulating to semiconducting and even superconducting states. This study emphasizes the synthesis of transition metal-doped TMDCs and investigates their integration as graphene-like materials to enhance optoelectronic functionalities. Furthermore, computational analyses are employed to predict and elucidate the properties of the doped structures, providing insights into their potential for next-generation optoelectronic applications.

Keywords: 2D materials, Graphene like materials, TMDC, Semiconductors, Optoelectronic devices, Light harvesting devices.

I. INTRODUCTION

Since the landmark discovery of graphene in 2004 [1], the field of two-dimensional (2D) materials has expanded rapidly, driven by their unique electronic, optical, mechanical, and catalytic properties [2,3]. While graphene's exceptional conductivity and transparency have positioned it as a key material, the limited bandgap restricts its direct application in photodetection. Consequently, research has shifted towards graphene analogues such as transition metal dichalcogenides (TMDs), black phosphorus, MXenes, and emerging III–V 2D semiconductors, which offer tunable bandgaps and rich optoelectronic functionalities [4–7]. Despite significant progress, the translation of these materials into practical photodetectors faces three core challenges:

Scalable Synthesis: Achieving high-quality, uniform, defect-free monolayers on an industrial scale remains elusive [8,9]. For example, while chemical vapor deposition (CVD) can produce large-area graphene, the transfer process introduces defects and contamination, impairing device performance.

Property Tunability & Functionalization: Precise control over doping, defect engineering, and heterostructure formation is necessary for optimizing responsivity, speed, and spectral range [10–12]. However, current methods often lack reproducibility and interface control.

Device Integration & Stability: Integrating these materials into heterostructures adds complexity, especially for air-sensitive materials like black phosphorus, which require encapsulation strategies [13–17].

Corresponding Author: Ahmed Abdelhady A. Khalil (a.abdelhady@niles.edu.eg)
Received April 21, 2025 Revised date: June 13, 2025 Accepted June 17, 2025

ISSN: 1687-8892

This review addresses a central question: How can different classes of 2D graphene-like materials overcome these barriers to enable practical applications in energy storage, catalysis, flexible electronics, and optoelectronics? By organizing the discussion around these three interrelated challenges, we shift from a purely descriptive overview to a critical analysis of material classes.

A comparative insight:

Table 1: Overview of material classes, synthesis approaches, limitations, and potential applications in photodetectors.

Material Class	Synthesis Approach	Major Limitation	Potential for Photodetector Application
Graphene	CVD, Mechanical exfoliation	Transfer-induced defects	High transparency, low resistance; limited bandgap
TMDs	CVT, Sulfurization	Uniformity at large scale	Adjustable bandgap, strong light-matter interaction
MXenes	Etching of MAX phases	Oxidation susceptibility	Metallic conductivity, tunable surface chemistry
Black Phosphorus	Mechanical exfoliation	Chemical instability	Direct bandgap, high mobility

Table (1) presents a comparative analysis of various material classes utilized in photodetector applications, highlighting their synthesis approaches, inherent limitations, and potential advantages. Graphene, synthesized via CVD and mechanical exfoliation, offers high transparency and low resistance but suffers from transfer-induced defects and a limited bandgap. Transition metal dichalcogenides (TMDs), obtained through CVT and sulfurization, provide adjustable bandgaps and strong light-matter interaction; however, achieving uniformity at a large scale remains a challenge. MXenes, derived by etching MAX phases, exhibit metallic conductivity and tunable surface chemistry but are highly susceptible to oxidation. Black phosphorus, produced through mechanical exfoliation, features a direct bandgap and high carrier mobility, though its chemical instability poses a significant limitation. The comparison underscores both the promising attributes and challenges of these materials in advancing photodetector technologies. A previous study presented the fabrication of Schottky and pn photodiodes using SiC/MoS_2 composite films via physical vapor deposition. The devices were structurally analyzed and electrically characterized. The vertical design enabled high efficiency, with the pn-diode achieving 14.68% EQE and 63.22 mA/W responsivity, while the Schottky diode reached 6.68% EQE and 28.25 mA/W. Response times were under 1 ms for both. The results highlight the potential of SiC/MoS_2 vertical structures for efficient optoelectronic applications [18]. Another paperwork reported the fabrication of a 1T-MoS_2-based pn photodiode using RF sputtering for fast photodetection. Structural analysis was performed using SEM and FTIR, while electrical performance was evaluated via I–V measurements from −2 to +2 V. The device achieved an EQE of 9.8%, an IQE of 10.5%, and a response time of 1.748 ms, demonstrating its suitability for rapid-response optoelectronic applications [19]. Recent studies have demonstrated that EQE of GaN/MoS_2 photodiodes can reach up to 11.86% in pn-junction configurations and 8.26% in Schottky device. Correspondingly, IQE has been reported to attain values of up to 13.78% and 10.02% for the pn- and Schottky-type photodiodes, respectively. Furthermore, response times have been observed to be approximately 800 µs for Schottky photodiode and 18.23 ms for pn-type device. [20].

II. GRAPHENE LIKE MATERIALS BASED PHOTODETECTOR PHOTONICS

2.1 Dynamic key performance parameters

To synthesize a light-harvesting apparatus, specifically a photodiode, it is imperative to comprehend the principal performance metrics that delineate its characteristics. The responsivity (R) of a photodetector serves as a quantitative parameter, defined as the ratio of the generated photocurrent to the incident power of electromagnetic radiation incident upon the device. This metric offers a direct representation of the efficacy with which the photodetector transduces optical power into an electrical current signal. the equation is defined as $R = \frac{I_{ph}}{P}$, where I_{ph} represents the photocurrent is delineated as the disparity observed between the current generated under illumination conditions and the current detected in the absence of illumination, commonly referred to as the dark current $(I_L - I_D)$, and P represents the power of the incident light. Within the realm of photovoltaic devices, an alternative definition of photo-responsivity can be considered. In this formulation, photo-responsivity is expressed as the ratio of the open-circuit voltage generated under illumination (V_p) to the power of the incident optical radiation (P). This alternative representation provides a measure of the photovoltaic conversion efficiency in terms of the voltage produced per unit of impinging optical power. This may be articulated as $R = \frac{V_p}{P}$. The spectral response range, wherein the responsivity decreases by 50%, corresponds to the interval of wavelengths encompassing the maximum and minimum currents. The noise equivalent power (NEP) denotes the minimum incident optical power required to yield a signal-to-noise ratio of unity at a frequency of 1 Hz. This metric serves as a measure of the ability of a photodetector to detect faint optical signals. Mathematically, the NEP can be represented as the quotient of the noise current (I_N) within a 1 Hz frequency bandwidth and the responsivity (R) of the photodetector $NEP = \frac{I_N}{R}$, where I_N represents the noise current within a frequency span of 1 Hz. Furthermore, the quantum efficiency (Q.E.)

refers to the proportion of charge carriers generated per incident photon. This parameter can be mathematically expressed as the ratio of the number of electrons produced at the output to the number of photons input to the device, denoted as $Q.E. = Electron\ Out/Photon\ In$. The power of light absorption at a given position z can be mathematically represented as:

$$P_z = P_{in}\ (1 - \mathcal{R})\ (1 - e^{-\alpha z}).$$

In this equation, where the incident power of light is denoted as Pin, the reflectivity of the material as R, the absorption coefficient of the material as α, and the distance from the surface as the variable z. The equation representing the number of photocarriers generated (η) by the illumination of individual photons may be expressed as:

$$\eta = (1 - \mathcal{R})\ (1 - e^{-\alpha d})$$

where d is the thickness of the active material with the maximum reflectivity $\mathcal{R}$. Furthermore, the detectivity (D) of a photodetector can be defined as the inverse of the noise equivalent power (NEP), expressed as $D = \frac{1}{NEP}$. The specific detectivity, also known as the spatially resolved detectivity, relates to the detectivity quantified within a designated unit area and across a frequency bandwidth of 1 Hz. It can be mathematically expressed as:

$$D = A_d B^{1/2} / NEP,$$

where A_d represents the area of the device and B denotes the bandwidth. Efficient detection of a weak signal becomes attainable through heightened localized detectivity exhibited by the photodetector. The photo-response time of a photodetector characterizes the temporal interval required for the device to convert incident optical radiation into an electrical signal, serving as a quantitative metric of its responsiveness. This parameter is evaluated through the measurement of both rise time (t_r) and fall time (t_f). The rise time denotes the duration for the electrical signal to transition from 10% to 90% of its steady-state value, whereas the fall time indicates the time required for the signal to transition from 90% to 10% of its steady-state value. These temporal metrics provide insight into the speed and efficiency with which the photodetector can respond to changes in the incident optical power. Both of these time measurements are essential in fully characterizing the photo-response capability of a gadget (Ahmed Abdelhady Khalil et al. 2024) [18-20]. The photoconductive gain (G) of a device can be defined as the quotient obtained by dividing the charge carrier lifetime associated with the generation of light and the transit time of the charge carriers as they drift through the device. Accordingly, the equation can be expressed as:

$$G = Carrier\ lifetime\ /\ Drift\ transit\ time$$

It is imperative to quantify this gain in order to assess the efficacy of the circulation of photogenerated carriers within the channel. The determination of G necessitates considering the transit time, which is contingent upon factors such as carrier mobility, the length of the device channel, and the magnitude of the applied voltage. The photoconductive gain can alternatively be quantified by the absorption power of light, denoted as P_{abs}. Understood, the gain (G) of the photodetector in this context can be expressed mathematically as: $G = (I_{ph}\ /P_{abs})\ (h\nu/\ q)$, where I_{ph} is the photocurrent generated by the device, where P_{abs} is the absorbed optical power, hν is the photon energy and q is the elementary unit of electric charge.

2.2 Graphene

Graphene, an allotrope of carbon, presents a two-dimensional structure defined by sp^2 hybridization. This hybridization process entails the amalgamation of atomic orbitals to generate novel hybrid orbitals, thereby modifying the electron configuration of the atom. Graphene has a hexagonal arrangement of carbon atoms, as depicted in Figure 1A by Roberts et al. (2010), This hexagonal lattice structure is referred to as a "honeycomb" lattice, the distinctive hexagonal arrangement of carbon atoms in graphene gives rise to its unusual and valuable electronic behavior, which is a key reason for the intense scientific and technological interest in this material [21], shows each atom forming strong covalent bonds with three neighboring atoms, with a distance of 0.142 nm between carbon atoms (Roberts et al., 2010) [21]. The valence and conduction bands of graphene overlap significantly at the Fermi level, resulting in pronounced symmetry (Berger et al., 2004) [22]. As a consequence of its monolayer atomic thickness and robust crystalline configuration, graphene exhibits distinctive attributes such as high carrier mobility, as highlighted by Brida et al. (2013) [23]. Concomitant with its single-layer atomic configuration and stable crystalline lattice structure, graphene exhibits a remarkably broad light absorption spectrum. This spectral range encompasses wavelengths spanning from the ultraviolet (UV) to the far-infrared (FIR) regions, and furthermore extends into the terahertz frequency domain, as elucidated in the work of Wang et al. (2008) [24]. Furthermore, studies have elucidated graphene's exceptional interactions with electromagnetic radiation, as detailed in the work of Iqbal et al. (2022) [25], Demonstrating an optical absorption rate of 2.3% across the visible and near-infrared spectral ranges (Nair et al., 2008) [26]. Moreover, through the modulation of its Fermi level, graphene has the capability to selectively absorb distinct wavelengths, rendering it highly efficient in photodetectors, notably in the mid-to-far-infrared wavelength spectrum. While graphene's zero-bandgap limits its direct usage in photodetection, strategies like doping and heterostructure formation can induce finite bandgaps. Recent developments focus on direct growth on flexible substrates to avoid transfer-induced defects [11].

Analytical insight:

Optimal synthesis involves balancing large-area uniformity with minimal defects, which directly correlates with device responsivity and noise characteristics.

2.3 Transition metal dichalcogenides (TMDCs)

Chemical vapor transport (CVT) and sulfurization techniques produce high-quality monolayers but face reproducibility issues over large areas [12,13].

Critical analysis:

Reproducibility of monolayer thickness and defect density remains a bottleneck, impairing spectral responsivity and response time consistency. TMDCs constitute a distinct class of semiconductor materials characterized by their layered architectures, which can consist of single or multiple layers arranged in a hexagonal symmetry. TMDCs are typically denoted by the general chemical formula MX_2, where M represents transition metal elements such as molybdenum (Mo), rhenium (Re), and tungsten (W), while X denotes chalcogen elements including sulfur (S), tellurium (Te), and selenium (Se). A multitude of TMDCs exhibit similar crystal structures, with notable examples including MoS_2, WS_2, and $MoSe_2$. TMDCs exhibit three primary structural phases: the trigonal prismatic (2H) phase, the distorted octahedral (1T) phase, and the dimerized (1T') phase are depicted in Figure 1B, as presented by Manzeli et al. in 2017 [27]. A considerable number of these patterns, specifically, exhibit a monolayer configuration resembling honeycomb structure, which can be further classified into distinct subcategories. Structures with trigonal prismatic geometry and D6h group symmetry are known as honeycomb (2H) structures, while those with distorted octahedral geometry and D3h group symmetry are referred to as centered honeycomb (1T) structures. (Ataca et al., 2012 [28]; Svetin et al., 2014 [29]; Manzeli et al., 2017 [27]).

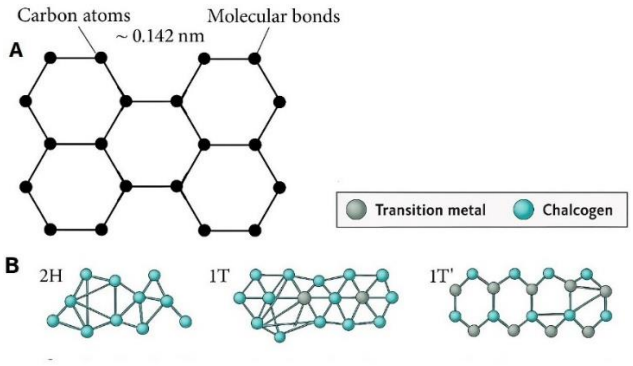

Figure 1 (A) Graphene structure (Roberts *et al.*, 2010) [21], and (B) Single layered atomic structure of TMDCs in trigonal prismatic phase (2H) distorted octahedral phase (1T) and dimerized phase (1T') states (Manzeli *et al*., 2017) [27].

Approximately 40 distinct types of transition metal dichalcogenide (TMDC) materials can be obtained by combining various chalcogenide elements with transition metals. The authors highlight a range of distinctive features, including specific charge density waves (Svetin et al., 2014) [30], semimetallic properties (Shishidou et al., 2001) [31], and notable superconductivity (Xi et al., 2016) [32]. In some instances, the expansion of relevant layers induces a transformation in the bandgap of monolayer MoS_2 from a direct bandgap of approximately 1.8 eV to an indirect bandgap of 1.2 eV in its bulk semiconductor form (Splendiani et al., 2010) [33]. In the context of group V layered dichalcogenides such as TaS_2, $TaSe_2$, and $NbSe_2$, it has been observed that charge density waves (CDWs) manifest within these materials, exhibiting a distinct phase. These waves are generated as a result of the presence of layers inside the material, the application of biassing, the deformation of substrates, and/or the stimulation of electric current. Several other topological semimetals, including $PtSe_2$, $PdTe_2$, and $PtTe_2$, exhibit remarkable chiral coupling transport properties alongside nonlinear optical characteristics (Fei et al., 2017) [34]. Additionally, these materials demonstrate peculiar physical properties, including unique carrier characteristics and wideband photodetection capabilities. The aforementioned features mostly arise from the electrical state being symmetrically insulated. In addition to other notable characteristics, TMDCs have a wide range of applications across multiple scientific disciplines. Several examples of these include optoelectronics, customizable excitonic devices, and spin-valley lasers (Ye et al., 2016a) [35].

2.4 MXenes & 2D Semiconductors

Etching methods for MXenes result in **layer control** but are hindered by **oxidation** [14]. Black phosphorus, with its direct bandgap, suffers from **ambient instability** [15].

Key future direction:

Developing protective encapsulation layers and in-situ growth methods will be critical to improve stability and uniformity.

2.5 Black Phosphorous

Black phosphorus (BP), a recently identified addition to the family of layered materials, exhibits a bandgap that is dependent on its thickness, ranging from 0.3 to 1.5 eV. This characteristic positions black phosphorus as a promising candidate for high-performance optoelectronic devices operating across the expansive infrared spectrum. Its 2D sheets can be seamlessly integrated with conventional materials like silicon (Youngblood et al., 2015) [36]. These sheets are also adaptable to various substrates, including flexible ones, as noted by Zhang et al. (2020) [37] and Qiao et al. (2014) [38]. Contrasted to other 2D materials, BP nanosheets display superior optical absorption, which mounts as the layer count drops Zhang et al. (2020) [37]; Qiao et al. (2014) [38]. Nevertheless, conventional BP photodetectors and solar cells realize challenges in detecting faint optical signals due to their inadequate responsivity, primarily studied in visible and near-infrared ranges (Liu et al., 2018 [39]; Ye et al., 2016b [40]). Unlike graphene, BP crystals have lower crystalline symmetry due to their puckered layer structure, resulting in asymmetric band structures that influence both electrical and optical conductivity (Shao et al., 2014 [41];

Wang and Lan, 2016 [42]). Figure 2 illustrates the multilayered 2D structure of BP (Shao et al., 2014) [41]. This structural asymmetry significantly impacts carrier transport characteristics. Research initiatives focused on BP-based photodetectors aim to enhance several key aspects: increasing responsivity, broadening spectral detection, minimizing dark current, improving time response, boosting the degree of sensitivity to polarization, and achieving waveguide integration.

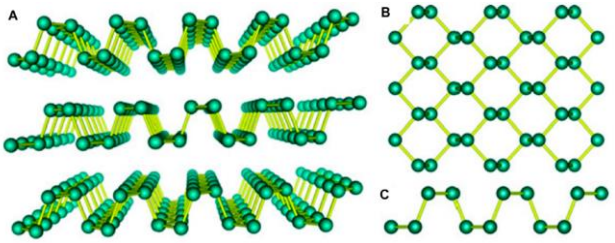

Figure 2 (A) black phosphorus multilayered crystal structure (Shao *et al*., 2014) [42], (B) Top view (Shao *et al*., 2014) [42], and (C) Side view (Shao *et al*., 2014) [42].

2.6 Group V-Based 2D-Materials

The anticipated growth of the 2D materials industry, especially those derived from group V elements, is expected to be significant, fueled by their versatility and potential for various electronic applications. This optimism stems from their notably high carrier mobility and adjustable bandgap, a feature notably absent in graphene and TMDCs, which typically exhibit indirect bandgaps, leading to diminished carrier mobility (Britnell et al., 2013 [43]; Zhang et al., 2016a [44]). Black phosphorus (BP) features a distinctive multilayered crystal structure composed of puckered honeycomb layers, akin to graphene. The layers are held together by weak van der Waals forces, resulting in anisotropic properties that make BP particularly intriguing for use in electronics and optoelectronics. Its direct bandgap crystal lattice structure promotes efficient light coupling, positioning black phosphorus as a promising candidate for a variety of optoelectronic applications, including photodetectors, sensors that cover the visible to mid-infrared ranges, and laser technologies (Shao et al., 2014 [41]; Iqbal et al., 2021c [45]). Additionally, tricyclic arsenene, characterized by notable stability and tunable bandgap, shows potential for optoelectronic devices due to its unique properties (Ma et al., 2016 [46]; Zhang et al., 2016a [44]). The anisotropic nature of 2D arsenic material, akin to black phosphorus, presents significant implications, surpassing even black phosphorus in this regard, enhancing its resilience compared to multilayered phosphorus. The application of ultra-thin layer samples on large surfaces offers practical advantages in preparation and application. While bulk antimony shares electrical transport traits with metals, its 2D layered form, with an indirect bandgap, poses challenges for optoelectronic devices despite its high carrier density and mobility (Zhang et al., 2016a [44]; Xie et al., 2016 [47]). The burgeoning interest in utilizing arsenic and antimony as emerging 2D stacked semiconductor materials across various device applications underscores their research significance (Zhang et al., 2016a; Xie et al., 2016) [47].

2.7 Group III-V Based 2D-Materials

Antimonides, including GaSb, InSb, AlSb, InAs, and their ternary and quaternary alloys, fall under the category of III-V semiconductors. The band alignments of these materials span a wide spectrum, ranging from type I to type III configurations (Vurgaftman et al., 2001) [48] driving the prevalent use of integrated photodetectors. Photodetectors utilizing scalable Ge have demonstrated high efficiency and maturity in sensing frequencies exceeding 67 GHz at a rate of 100 Gigabauds (GBd) (Chen et al., 2016) [49]. Many III-V materials exhibit higher absorptivity and can directly adjust the bandgap, making them ideal for efficient operation in optical sensing devices like lasers (Staudinger, 2020) [50] and LEDs (Li et al., 2019) [51].

III. DEVICE ARCHITECTURE AND PERFORMANCE METRICS

3.1 Device Structures

Vertical heterostructures (e.g., graphene/TMD) have demonstrated high responsivity due to efficient charge separation [16].

Comparison:

Vertical stacking improves photoresponsivity but introduces interface resistance; lateral junctions offer better control but are harder to scale.

3.2 Critical Metrics and Limitations

Table 2: Overview of device parameters, current performance, and key limitations impacting responsivity, response time, and noise-equivalent power.

Parameter	Current State	Limitation
Responsivity	Up to 1000 A/W in optimized heterostructures [17]	Interface quality limits efficiency
Response Time	Sub-millisecond responses possible [18]	Trade-offs between responsivity and speed
Noise EQ Power	Decreasing with material quality	Needs further reduction by interface engineering

Table (2) provides an overview of key performance parameters for photodetectors, highlighting their current capabilities and associated limitations. Responsivity, which measures the efficiency of light conversion into electrical signals, can reach up to 1000 A/W in optimized

heterostructures; however, interface quality remains a limiting factor in achieving higher efficiency. Response time, crucial for fast detection, can be reduced to sub-millisecond levels, but there is an inherent trade-off between speed and responsivity. Noise equivalent power (NEP), a metric indicating sensitivity, has been decreasing with improvements in material quality, yet further reductions are necessary through interface engineering to enhance overall performance. This summary underscores the challenges and opportunities in advancing photodetector technologies.

Future Directions

- Hybrid materials combining high responsivity and stability.
- Interface engineering to reduce contact resistance and trap states.
- Encapsulation for air-sensitive materials.

IV. 2D-MATERIALS BASED PHOTODETECTORS

4.1 Graphene based photodetectors

Graphene, a two-dimensional material characterized by its hexagonal structure, demonstrates optical absorption within a limited spectral range due to its extremely thin thickness. The photoresponsivity of the device is somewhat restricted, as indicated by a value of 0.5 mA/W and a bandwidth of 500 GHz, as reported by Mueller et al. (2010) [52]. According to reports, photodetectors composed of metal-graphene-metal structures featuring asymmetric electrodes demonstrate a notable responsivity of 6.1 mA/W. The aforementioned outcome stands in opposition to the exceptional characteristics of graphene, such as its remarkable velocity, compatibility with circuits, and versatility across a broad range of frequencies (Lou et al., 2016) [53]. Several solutions have been proposed thus far to enhance the optical absorption capabilities of graphene photodetectors. One such approach involves the utilization of nanostructured plasmonics. This technique enhances the concentration of light and can be effectively employed for achieving multicolor detection while also improving the quantum efficiency of the device. According to a study conducted by Fang et al. (2012) [54], it has been observed that incorporating plasmonic nano-antennas within the layers of a graphene photodetector can significantly enhance its quantum efficiency, reaching up to 20%. Additionally, by controlling the resonance of these nanostructures, it is possible to manipulate the operational bandwidth of the device. Another approach to improve the photoresponsivity involves the integration of quantum dots (QDs) into graphene. According to the methodology employed, the photoresponsivity seen in photodetection exhibits a greater value, specifically reported to range between 10^7 and 10^8 A/W, as indicated by Konstantatos et al. (2012) [55]. The aforementioned phenomena enables the efficient transfer of photo-excited carriers to the graphene layer, while simultaneously trapping carriers of opposite charge due to the field-effect doping effect. The utilization of PbS-QDs has been observed in graphene photodetectors, with a claimed photoresponsivity of 10^7 A/W (Sun et al., 2012) [56]. An alternative strategy that has demonstrated efficacy involves the utilization of photodetectors based on graphene QDs within microcavities, resulting in enhanced photoactivity in graphene with reduced operational speed and bandwidth limitations (Gan et al., 2013) [57]. The device has a pretty high level of response speed. Moreover, it demonstrates exceptional efficiency, an extensive range of bandwidth, and heightened light responsivity. Nevertheless, the dimensions of the device are greater compared to traditional photodetectors, which is identified as a significant limitation (Kim et al., 2011) [58]. The study focused on investigating the bolometric responses of single-layer graphene (SLG) under ambient temperature conditions by applying bias. This observation unveils two distinct mechanisms that contribute to the generation of polarized bolometric photocurrents: (1) the augmentation of conductance through the introduction of light-induced carriers, and (2) the reduction in conductance resulting from the temperature dependence of carriers. The dominant mechanisms in systems influenced by varying electric fields are photovoltaic (PV) effects, particularly when the carrier density is notably low. In the context of ambient-temperature graphene bolometric detectors, it has been observed that photo-thermoelectric (PTE) effects play a significant role. Additionally, Freitag et al. (2013) reported a photoresponsivity of 0.2 mA/W [59]. To address this issue, Yan et al. (2012) [60] utilized a bi-layer graphene (BLG) structure that incorporates a dual gate configuration, including an anti-reflective top gate (Koppens et al., 2014) [61]. The device was measured using a four-terminal configuration while being exposed to mid-infrared (MIR) radiation at a wavelength of 10.6 micrometers. The detection of light response was achieved using a bolometric mechanism, as described by Liu et al. (2013) [62]. Although this system is typically examined using radiofrequency waves, it is also applicable to optical detection (Vora et al., 2012) [63]. Graphene is a favorable choice for room-temperature photodetection applications due to its notable attributes, including enhanced mobility, reduced carrier transit time, and heightened susceptibility to electrostatic perturbations from photogenerated surface carriers. Colloidal quantum dots (QDs) synthesized using PbS, as demonstrated by Sun et al. (2012) [56], Jeong et al. (2020) [64] and Konstantatos et al. (2012) [55], serve as examples of light-absorbing particles sensitized by graphene. Detecting photons under low incident light intensities, particularly at the single-photon level, requires a gain mechanism that generates a large number of electrical carriers in response to each photon. This objective can be achieved through deliberate modification of the surface properties to enhance light absorption capabilities, thereby facilitating the effective passage of charge carriers into the conductor. This phenomenon is observed alongside a modification in the resistance versus

gate-voltage relationship, (Konstantatos et al. in 2012) [55].

4.2 TMDCs based photodetectors

TMDCs such as MoS_2, $MoSe_2$, WS_2, WSe_2, ReS_2, $ReSe_2$, and $MoTe_2$, reveal promising characteristics for photodetection applications. MoS_2's monolayered and few-layered configurations possess high charge carrier mobility (~200 $cm^2V^{-1}s^{-1}$), a direct bandgap of 1.8 eV, efficient current on/off ratios, and improved light-matter interaction (Splendiani et al., 2010 [65]; George et al., 2021 [66]; Ponomarev et al., 2015 [67]). George et al. (2021) [66] stated the discovery of a robust and sizable persistent photoconductor, called the gigantic persistent photoconductor (GPPC), fabricated via chemical vapor deposition (CVD) of monolayer MoS_2, displaying improved conductivity up to a factor of 10^7 when operated at 365 nm. Yin et al. (2012) [68] employed MoS_2 nanosheets in a transistor arrangement, exhibiting a responsivity of 75 mA/W and a response speed of 50 ms at a wavelength of 670 nm. Lopez-Sanchez et al. (2013) [69] enhanced the MoS_2 monolayer device, attaining a responsivity of 800 mA/W at 680 nm. $MoSe_2$, with its significant photoluminescence and direct bandgap of 1.5 eV, has been investigated for photodetection (Zhang et al., 2014a) [70]. Synthesis methods like chemical vapor deposition (CVD) and exfoliation have superior device performance (Abderrahmane et al., 2014 [71]; Lu et al., 2014 [72]). Wang et al. afforded a widespread overview of 2D materials in the background of photodetection applications (Wang et al., 2018) [73], whereas Xia et al. supervised a study on a photodetector based on $MoSe_2$ (Xia et al., 2014a) [74]. For $MoSe_2$, Zhang et al. (2013a) [75] synthesized a monolayer phototransistor, demonstrating higher responsivity compared to multilayered devices.

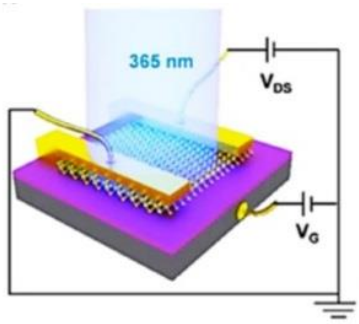

Figure 3 MoS_2 single-layered phototransistor Schematic (George et al., 2021) [66].

On the contrary, the application of CVD to fabricate multilayered $MoSe_2$ devices has been found to demonstrate improved responsivity. However, it is important to note that this improvement in responsivity is accompanied by a reduction in response speed, as reported by Jung et al. in 2015 [76]. Similarly, exfoliated $MoSe_2$ photodetectors exhibited improved responsivity (Abderrahmane et al., 2014) [71]. WS_2 photodetector, which belongs to the family of TMDC materials, has been successfully synthesized by various methodologies as documented by Sik Hwang et al. in 2012 [77]. WS_2 photodetectors synthesized via various methods have demonstrated responsivity correlated with photon energy, reaching 92 μA/W with a response speed of 5 ms within a wavelength range of 457–647 nm (Perea-López et al., 2013) [78]. The researchers demonstrated a correlation between photon energy and their detectors, as evidenced by the measured device responsivity of 92 μA/W and response speed of 5 ms, which were obtained within an operating wavelength range of 457–647 nm. Additionally, the utilization of WSe_2, characterized by its single-layer and multilayered structures, has been extensively examined in photodetection applications. In a study by Zhang et al. (2014b) [79], chemical vapor deposition (CVD) was employed to synthesize a monolayered WSe_2 device. The investigation into the effect of varying the work function in metal contacts revealed that the Pd contact achieved the highest responsivity of 1.8×10^5 A/W at an operating wavelength of 650 nm, while the Ti contact exhibited the lowest device responsivity. The Titanium (Ti) contact displayed an efficient response time of 23 ms, which is longer than that of other metal contacts. This delay can be attributed to the presence of a Schottky contact between the active materials, underscoring the importance of improving metal contact performance to enhance device efficacy. $MoTe_2$ has garnered significant interest due to its intriguing optoelectronic properties (Lin et al., 2014) [80]. TMDs like ReS_2 and $ReSe_2$ have a layered structure similar to black phosphorus. These materials demonstrate interesting properties due to their anisotropic nature, impacting their bandgap and carrier mobilities. Such characteristics play a significant role in determining the performance of devices based on these materials, like transistors and photodetectors. (Wilson and Yoffe, 1969 [81]; Yang et al., 2014 [82]). $ReSe_2$ devices have demonstrated a responsivity of 95 A/W and rapid response time at 633 nm (Yang et al., 2014) [82]. Despite their efficacy, TMDC-based photodetectors exhibit environmental sensitivity, influencing device performance (Jo et al., 2016) [83]. Encapsulation passivation techniques can mitigate this sensitivity (Jo et al., 2016) [83]. The utilization of encapsulation passivation techniques can effectively reduce the device's reliance on external factors, hence improving its overall efficiency. While $ReSe_2$ has demonstrated efficacy as a photodetection device, it is accompanied with a limitation whereby the current flow does not revert back to its original dark current level under low-light conditions. The observed phenomenon can be ascribed to the sluggish recombination of charge carriers, a characteristic that has been substantiated by the application of brief pulses to the gate terminals to reset the device (Konstantatos et al., 2012 [55]; Ahn et al., 2021 [84]). In the study by Liu et al. (2016a) on ReS_2 photodetectors detecting polarized light at an operational wavelength of 1064 nm, the responsivity values ranged from 3.97×10^3 to 1.18×10^6 A/W. The enhancement in responsivity for specific polarizations could be linked to electron doping, as depicted in Figure 3B of their research. This electron doping process likely plays a significant role in the observed improvement in detecting polarized light using ReS_2 photodetectors [85]. TMDCs can function as

photodiodes or photoconductors under appropriate biasing conditions (Lopez-Sanchez et al., 2013) [86]. Integration of TMDCs with graphene electrodes has shown potential for efficient current generation (Koppens et al., 2014) [61]. Additionally, WS_2-based flexible photodetectors demonstrated high photoresponsivity (Li et al., 2020) [86]. The Graphene-WS_2-Graphene configuration showed enhanced detectivity and photoresponsivity (Pham et al., 2022) [87]. TMDC-based photodetectors generally exhibit responsivity between 10^{-7} and 10^{7} A/W and response times ranging from 10^{-5} to 10^{3} s, with improved responsivity observed near material traps or interfaces (Pham et al., 2022) [87]. Optimization of device performance considers synthesis methods, environment, and layer count (Pham et al., 2022) [87].

V. PHOTODETECTORS IN VISIBLE AND NIR REGIONS

Photodetectors operating in the visible and near-infrared (IR) spectrum are crucial for various applications, and graphene-based devices have shown promise in this regard. Graphene photodetectors, in conjunction with metal electrodes, can efficiently separate charge carriers, resulting in a responsivity of up to 6.1 mA/W as shown in Figure 4 (A) (Mueller et al., 2010) [52]. Additionally, vertically stacked layer graphene devices with metal contacts exhibit wavelength-dependent performance, leveraging the carrier multiplication effect (Chen et al., 2015) [88]. Despite its lack of a bandgap, graphene is complemented by 2D transition metal dichalcogenides (TMDCs) like MoS_2, $MoSe_2$, WS_2, WSe_2, ReS_2, and $ReSe_2$, which have shown efficiency in photodetection applications (Mukherjee et al., 2015 [89]; Zhang et al., 2016c [90]).

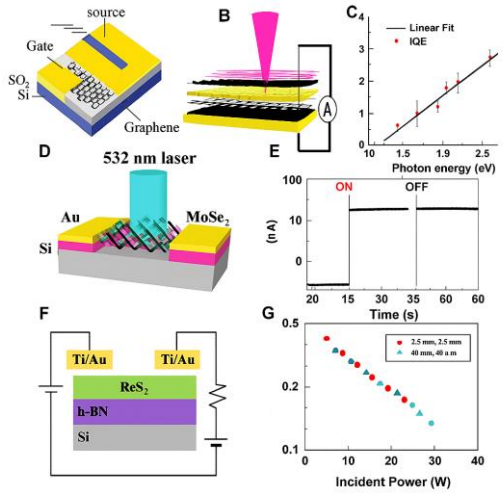

Figure 4 (A) Graphene photodetector with different metal contacts Mueller *et al*. (2010) [52], (B) graphene configuration where multiple layers are stacked on top of each other Chen *et al*. (2015) [88], (C) graphene optical properties based on photon energy dependence such as IQE, (D) Monolayered $MoSe_2$ photodetector Wang *et al*. (2018) [73], (E) With its time resolved current Wang *et al*. (2018) [73], (F) Multilayered $ReSe_2$ photodetector Liu *et al*. (2016a), and (G) With its responsivity Liu *et al*. (2016a) [85].

The bulk form of MoS_2 has an indirect bandgap of 1.2 eV, which can be altered to 1.8 eV by transforming the material into a nanosheet or thin film configuration. The material has favorable characteristics for near-infrared (NIR) detection, including a low dark current and a high on/off ratio. This is attributed to its strong compatibility with the incident NIR wavelength light, as demonstrated in studies conducted by Lopez-Sanchez et al. (2013) [70], Radisavljevic et al. (2011) [91], Ehsan Elahi et al. (2024) [92], V. Janardhanam et al. (2023) [93] and M. Malik et al. (2022) [28]. According to a study conducted by Lopez-Sanchez et al. in 2013 [69], photodetectors based on single-layered MoS_2 demonstrate a responsivity of 880 A/W when operated at a wavelength of 561 nm. The utilization of $MoSe_2$ in spintronics is advantageous due to its notable spin splitting energy. The material under investigation exhibits a comparatively longer response time when compared to the MoS_2 devices as seen in Figures 4D and E (Wang et al., 2018) [73]. In their study, Liu et al. successfully produced a photodetector based on multilayered ReS_2. They demonstrated that this photodetector had a response of 88600 A/W at a specific operating wavelength of 532 nm, as illustrated in Figures 4F and G (Liu et al., 2016a) [85]. The efficiency of this reaction is higher in comparison to that of the device based on single-layered RSe_2.

VI. GAPS, CHALLENGES, AND FUTURE OUTLOOK

Despite progress, scalability remains the overarching challenge. To bridge lab-scale demonstrations and industrial applications, focus should be on:

- Scalable synthesis techniques: Roll-to-roll CVD, ALD, and direct growth methods.
- Material stabilization: Encapsulation and surface passivation.
- Heterostructure engineering: Precise control over interfaces for optimized carrier dynamics.

6.1 Proposed research directions:

- Developing high-throughput synthesis for uniform 2D layers.
- In-situ characterization during growth for real-time quality control.
- Exploring novel heterostructures that combine the strengths of different materials.

6.2 Future Outlook:

Advancing bottom-up synthesis techniques—such as molecular beam epitaxy (MBE) and atomic layer deposition (ALD)—coupled with interface engineering, will be essential to realize scalable, high-quality 2D photodetectors.

VII. CONCLUSION

The field of optoelectronics places considerable emphasis on the investigation of photodetectors, particularly those derived from TMDCs. While photovoltaics and light-emitting devices also receive attention, they are less prominent in comparison. As the demand for data-intensive models and connectivity grows, there is an increasing need for innovative approaches to implement additional features.

A critical factor influencing device performance is the fabrication of high-quality ohmic contacts to TMDCs, particularly for mono- to tri-layer flakes. Understanding the metal connections to TMDCs and minimizing resistance in these connections are essential for optimizing performance in optoelectronic and photonic devices. The unique material properties of TMDCs render them highly suitable for flexible electronic applications. Therefore, it is crucial to thoroughly investigate their interactions with flexible organic substrates and their compatibility with flexible device processing.

In terms of device design and future technology, it is important to prioritize straightforward operation over complex designs to meet performance objectives effectively. Additionally, secondary factors such as thermal losses, heat dissipation, external noise, and related aspects should be considered when analyzing device performance.

Bridging the gap between research and the development of commercial products utilizing TMDCs requires effective collaboration between academia and industry. Such partnerships will facilitate the translation of research findings into practical applications, driving innovation and progress in the field of TMDC-based devices.

Achieving scalable, high-quality synthesis and robust device integration are vital to elevate 2D materials from laboratory curiosities to practical photodetectors. Future research must prioritize reproducibility, stability, and interface control to unlock their full potential for applications spanning from flexible electronics to high-speed optical communications.

Acknowledgments:

The authors wish to express their deepest appreciation to National institute of Laser Enhanced Sciences (NILES), Cairo University, and the American University in Cairo (AUC) for their exceptional support and encouragement throughout this research. The invaluable assistance provided by both institutions has been instrumental in the successful completion of this study, and their unwavering commitment to academic excellence has greatly inspired us.

Author contributions:

All authors contributed to the conception and design of the study. Material preparation and data collection were performed by Ahmed Abdelhady A. Khalil. Figures (1-4) were prepared by Heba A. Shawkey. All authors reviewed the manuscript. The first draft was written by Ahmed Abdelhady A. Khalil, Samar Akef, Heba A. Shawkey, and Mohamed A. Swillam, with all authors providing comments on previous versions. All authors read and approved the final manuscript. The revisions were made by Ahmed Abdelhady A. Khalil, Samar Akef, and Mohamed A. Swillam.

Funding and/or Competing interests:

The authors declare that no funds, grants, or other support were received during the preparation of this manuscript.

The authors have no competing interests to declare that are relevant to the content of this article.

Data Availability Statement:

Data Availability Statement: No Data associated in the manuscript.

REFERENCES

1. Novoselov, K. S., et al. Electric field effect in atomically thin carbon films. Science, (2004); 306(5696), 666–669.
2. Chhowalla, M., et al. The chemistry of two-dimensional layered transition metal dichalcogenide nanosheets. Nature Chemistry, (2013); 5(4), 263–275.
3. Akinwande, D., et al. A review on mechanics and mechanical properties of 2D materials—Graphene and beyond. Extreme Mechanics Letters, (2017); 13, 42–77.
4. Wang, Q. H., et al. Electronics and optoelectronics of two-dimensional transition metal dichalcogenides. Nature Nanotechnology, (2012); 7(11), 699–712.
5. Naguib, M., et al. Two-dimensional nanocrystals produced by exfoliation of Ti_3AlC_2. Advanced Materials, (2011); 23(37), 4248–4253.
6. Liu, H., et al. . Phosphorene: an unexplored 2D semiconductor with a high hole mobility. ACS Nano, (2014); 8(4), 4033–4041.
7. Vogt, P., et al. Silicene: Compelling experimental evidence for graphenelike two-dimensional silicon. Physical Review Letters, (2012); 108(15), 155501.
8. Lin, Z., et al. A scalable CVD approach for the synthesis of 2D materials. Nature Reviews Materials, (2021); 6(6), 391–411.
9. Ghosh, R., et al. Roll-to-roll production of large-area 2D materials: status and prospects. Advanced Materials, (2023); 35(20), 2207320.
10. Voiry, D., et al. Phase engineering of transition metal dichalcogenides. Chemical Society Reviews, (2015); 44(9), 2702–2712.
11. Dong, Y., et al. Surface functionalization of MXenes for tunable electrochemical properties. ACS Nano, (2022); 16(2), 2290–2304.
12. Zhang, Y., et al. Doping strategies in 2D materials for electronics and energy. Chemical Society Reviews, (2020); 49(21), 7339–7376.
13. Kang, K., et al. High-mobility three-atom-thick semiconducting films with wafer-scale homogeneity. Nature, (2015); 520(7549), 656–660.

14. Li, X., et al. . Integration of 2D materials into CMOS-compatible platforms. 3Nature Electronics, (2023); 6(3), 154–164.
15. Bonaccorso, F., et al. 2D materials: Getting ready for the market. Nature Nanotechnology, (2015); 10(9), 780–783.
16. Lee, Y., et al. . Industrial-scale challenges in 2D materials: From synthesis to system integration. Nature Materials, (2023); 22(2), 142–153.
17. Li, Y., et al. 2D materials in practical applications: a roadmap. Advanced Functional Materials, (2024); 34(5), 2309802.
18. Khalil Ahmed Abdelhady A., Karmalawi Abdallah M., Abdelmageed Alaaeldin A., et al. Thin-film photodiode based on novel SiC/MoS_2 composite by RF-sputtering for fast response photodetection. Optical Materials, (2024); 150 : 115168.
19. Khalil Ahmed Abdelhady A., Karmalawi Abdallah M., Abdelmageed Alaaeldin A., et al. Fast response fabricated MoS_2-photodiode based thin film. Journal of Materials Science: Materials in Electronics, (2024); 35, 8 : 546.
20. Khalil Ahmed Abdelhady A., Karmalawi Abdallah M., Abdelmageed Alaaeldin A., et al. Impact behavior of a novel GaN/MoS_2 composite photodiode based thin-film by RF-sputtering for fast response photodetection application. Optical and Quantum Electronics, (2024); 56, 5: 804.
21. Roberts, M. W., Clemons, C. B., Wilber, J. P., et al. Continuum Plate Theory and Atomistic Modeling to Find the Flexural Rigidity of a Graphene Sheet Interacting with a Substrate. J. Nanotechnol., (2010).
22. Berger, C., Song, Z., Li, T., et al. Ultrathin Epitaxial Graphite: 2DElectron Gas Properties and a Route toward Graphene-Based Nanoelectronics. J. Phys. Chem. B, (2004); 108 (52), 19912–19916.
23. Brida, D., Tomadin, A., Manzoni, C., et al. Ultrafast Collinear Scattering and Carrier Multiplication in Graphene. Nat. Commun. (2013); 4 (1), 1987–1989.
24. Wang, F., Zhang, Y., Tian, C., et al. Gate variable Optical Transitions in Graphene. Science, (2008); 320 (5873), 206–209.
25. Iqbal, M. A., Malik, M., Shahid, W., et al. . Materials for Photovoltaics: Overview, Generations, Recent Advancements and Future Prospects. Thin Films Photovoltaics, (2022); 5.
26. Nair, R. R., Blake, P., Grigorenko, A. N., et al. Fine Structure Constant Defines Visual Transparency of Graphene. Science, (2008); 320 (5881), 1308.
27. Manzeli, S., Ovchinnikov, D., Pasquier, D., et al. 2D Transition Metal Dichalcogenides. Nat. Rev. Mater., (2017); 2 (8), 1–5.
28. Malik, M., Iqbal, M. A., Choi, J. R, et al. 2D materials for efficient photodetection: Overview, mechanisms, performance and UV-IR range applications. Frontiers in Chemistry, (2022); 10 : 905404.
29. Ataca, C., Şahin, H., and Ciraci, S. Stable, Single-Layer MX_2 Transition-Metal Oxides and Dichalcogenides in a Honeycomb-like Structure. J. Phys. Chem. C, (2012); 116 (16), 8983–8999.
30. Svetin, D., Vaskivskyi, I., Sutar, P., et al. Transitions between Photoinduced Macroscopic Quantum States in 1T TaS_2 controlled by Substrate Strain. Appl. Phys. Express, (2014); 7 (10), 103201.
31. Shishidou, T., Freeman, A. J., and Asahi, R. Effect of GGA on the Half-Metallicity of the Itinerant ferromagnet CoS_2. Phys. Rev. B, (2001); 64 (18), 180401.
32. Xi, X., Wang, Z., Zhao, W., et al. Ising Pairing in Superconducting $NbSe_2$ Atomic Layers. Nat. Phys. (2016); 12 (2), 139–143.
33. Splendiani, A., Sun, L., Zhang, Y., et al. Emerging Photoluminescence in Monolayer MoS_2. Nano Lett., (2010);10 (4), 1271–1275.
34. Fei, F., Bo, X., Wang, R., et al. Nontrivial Berry Phase and Type-II Dirac Transport in the Layered Material $PdTe_2$. Phys. Rev. B, (2017); 96 (4), 041201.
35. Ye, L., Li, H., Chen, Z., et al. Near-Infrared Photodetector Based on MoS_2/Black Phosphorus Ð Heterojunction. Acs Photonics, (2016); 3 (4), 692–699.
36. Youngblood, N., Chen, C., Koester, S. J., et al. Waveguide-integrated Black Phosphorus Photodetector with High Responsivity and Low Dark Current. Nat. Phot., (2015); 9 (4), 247–252.
37. Zhang, G., Huang, S., Wang, F., et al. The Optical Conductivity of Few-Layer Black Phosphorus by Infrared Spectroscopy. Nat. Commun., (2020); 11 (1), 1847.
38. Qiao, J., Kong, X., Hu, Z. X., et al. High-mobility Transport Anisotropy and Linear Dichroism in Few-Layer Black Phosphorus. Nat. Commun. (2014); 5 (1), 4475–4477.
39. Liu, L., Sun, T., Ma, W. et al. Highly Responsive Broadband Black Phosphorus Photodetectors. China Opt. Express, (2018); 16 (2), 020002.
40. Ye, Y., Xiao, J., Wang, H., et al. Electrical Generation and Control of the Valley Carriers in a Monolayer Transition Metal Dichalcogenide. Nat. Nanotech, (2016); 11 (7), 598–602.
41. Shao, D. F., Lu, W. J., Lv, H. Y., et al. Electron-doped Phosphorene: a Potential Monolayer Superconductor. Europhysics Letters, (2014); 108, 67004.
42. Wang, X., and Lan, S. Optical Properties of Black Phosphorus. Adv. Opt. Phot. (2016); 8 (4), 618–655.
43. Britnell, L., Ribeiro, R. M., Eckmann, A., et al. Strong Light-Matter Interactions in Heterostructures of Atomically Thin Films. Science, (2013); 340 (6138), 1311–1314.
44. Zhang, S., Xie, M., Li, F., et al. Semiconducting Group 15 Monolayers: a Broad Range of Band Gaps and High Carrier Mobilities. Angew. Chem., (2016); 128 (5), 1698–1701.
45. Iqbal, M. A., Ashraf, N., Shahid, W., et al. Nanophotonics: Fundamentals, Challenges, Future Prospects and Applied Applications, (2021).
46. Ma, S., Zhou, P., Sun, L. Z., et al. Two-dimensional Tricycle Arsenene with a Direct Band Gap. Phys. Chem. Chem. Phys., (2016); 18 (12), 8723–8729.
47. Xie, M., Zhang, S., Cai, B., et al. A Promising Two-Dimensional Solar Cell Donor: Black Arsenic-Phosphorus Monolayer with 1.54 eV Direct Bandgap and Mobility Exceeding 14,000 $cm^2V^{-1}s^{-1}$. Nano Energy, (2016); 28, 433–439.

48.Vurgaftman, I., Meyer, J. R., and Ram-Mohan, L. R. Band Parameters for III-V Compound Semiconductors and Their Alloys. J. Appl. Phys., (2001); 89 (11), 5815–5875.
49.Chen, H., Galili, M., Verheyen, P., et al. 100-Gbps RZ Data Reception in 67-GHz Si-Contacted Germanium Waveguide Pin Photodetectors. J. Light. Technol., (2016); 35 (4), 722–726.
50.Staudinger, P. Crystal Phase Engineering in III-V Semiconductor Films: From Epitaxy to Devices. Lausanne: EPFL, (2020).
51. Li, N., Han, K., Spratt, W., et al. Ultra-low power Sub-photon-voltage High-Efficiency Light-Emitting Diodes. Nat. Photonics, (2019); 13 (9), 588–592.
52.Mueller, T., Xia, F., and Avouris, P. Graphene Photodetectors for High-Speed Optical Communications. Nat. Phot., (2010); 4 (5), 297–301.
53. Lou, Z., Liang, Z., and Shen, G. Photodetectors Based on Two Dimensional Materials. J. Semicond, (2016); 37 (9), 091001.
54. Fang, Z., Liu, Z., Wang, Y., et al. Graphene-antenna Sandwich Photodetector. Nano Lett., (2012);12 (7), 3808–3813.
55. Konstantatos, G., Badioli, M., Gaudreau, L., et al. Hybrid Graphene-Quantum Dot Phototransistors with Ultrahigh Gain. Nat. Nanotech, (2012); 7 (6), 363–368.
56. Sun, Z., Liu, Z., Li, J., et al. . Infrared Photodetectors Based on CVD-Grown Graphene and PbS Quantum Dots with Ultrahigh Responsivity. Adv. Mat., (2012); 24 (43), 5878–5883.
57. Gan, X., Shiue, R.-J., Gao, Y., et al. Chip integrated Ultrafast Graphene Photodetector with High Responsivity. Nat. Phot., (2013); 7 (11), 883–887.
58. Kim, K., Choi, J.-Y., Kim, T., et al. A Role for Graphene in Silicon-Based Semiconductor Devices. Nature, (2011); 479 (7373), 338–344.
59. Freitag, M., Low, T., Xia, F., et al. Photoconductivity of Biased Graphene. Nat. Phot. (2013); 7 (1), 53–59.
60. Yan, J., Kim, M.-H., Elle, J. A., et al. Dual-gated Bilayer Graphene Hot-Electron Bolometer. Nat. Nanotech, (2012); 7(7), 472–478.
61. Koppens, F. H. L., Mueller, T., Avouris, P., et al. Hybrid Graphene–Quantum Dot Phototransistors with Ultrahigh Gain. Nat. Nanotech., (2014); 7 (6), 363–368.
62. Liu, G., Ahsan, S., Khitun, A. G., et al. Graphene based Non-Boolean Logic Circuits. J. Appl. Phys., (2013); 114 (15), 154310.
63.Vora, H., Kumaravadivel, P., Nielsen, B., et al. Bolometric Response in Graphene Based Superconducting Tunnel Junctions. Appl. Phys. Lett., (2012); 100 (15), 153507.
64. Jeong, H., Song, J. H., Jeong, S., et al. Graphene/PbS Quantum Dot Hybrid Structure for Application in Near-Infrared Photodetectors. Sci. Rep., (2020); 10 (1), 12475–12477.
65. Splendiani, A., Sun, L., Zhang, Y., et al. Emerging Photoluminescence in Monolayer MoS_2. Nano Lett., (2010); 10 (4), 1271–1275.
66. George, A., Fistul, M. V., Gruenewald, M., et al. Giant Persistent Photoconductivity in Monolayer MoS_2 Field-Effect Transistors. npj 2D Mater. Appl., (2021); 5 (1), 1–8.
67. Ponomarev, E., Gutiérrez-Lezama, I., Ubrig, N., et al. Ambipolar Light-Emitting Transistors on Chemical Vapor Deposited Monolayer MoS_2. Nano Lett., (2015); 15 (12), 8289–8294.
68.Yin, Z., Li, H., Li, H., et al. Single-Layer MoS_2 Phototransistors. ACS Nano, (2012); 6 (1), 74–80.
69. Lopez-Sanchez, O., Lembke, D., Kayci, M., et al. Ultrasensitive Photodetectors Based on Monolayer MoS_2. Nat. Nanotech, (2013); 8 (7), 497–501.
70. Zhang, W., Chiu, M.-H., Chen, C.-H., et al. Role of Metal Contacts in High-Performance Phototransistors Based on WSe_2 Monolayers. ACS Nano, (2014); 8 (8), 8653–8661.
71.Abderrahmane, A., Ko, P. J., Thu, T. V., et al. High Photosensitivity Few-Layered $MoSe_2$ Back-Gated Field-Effect Phototransistors. Nanotechnology, (2014); 25 (36), 365202.
72. Lu, X., Utama, M. I. B., Lin, J., et al. Large-Area Synthesis of Monolayer and Few-Layer $MoSe_2$ Films on SiO_2 Substrates. Nano Lett., (2014); 14 (5), 2419–2425.
73. Wang, G., Zhang, Y., You, C., et al. Two Dimensional Materials Based Photodetectors. Infrared Phys. Technol. (2018); 88, 149–173.
74. Xia, F., Wang, H., and Jia, Y. Rediscovering Black Phosphorus as an Anisotropic Layered Material for Optoelectronics and Electronics. Nat. Commun., (2014); 5 (1), 4458–4466.
75. Zhang, W., Huang, J.-K., Chen, C.-H., et al. High-Gain Phototransistors Based on a CVD MoS_2 Monolayer. Adv. Mat., (2013); 25 (25), 3456–3461.
76. Jung, C., Kim, S.M., Moon, H., et al. Highly Crystalline CVD-Grown Multilayer $MoSe_2$ Thin Film Transistor for Fast Photodetector. Sci. Rep., (2015); 5 (1), 15313–15319.
77. Sik Hwang, W., Remskar, M., Yan, R., et al. Transistors with Chemically Synthesized Layered Semiconductor WS_2 Exhibiting 105 Room Temperature Modulation and Ambipolar Behavior. Appl. Phys. Lett., (2012); 101 (1), 013107.
78. Perea-López, N., Elías, A. L., Berkdemir, A., et al. Photosensor Device Based on Few-layered WS_2 Films. Adv. Funct. Mater., (2013); 23 (44), 5511–5517.
79.Zhang, Y., Chang, T.-R., Zhou, B., et al. Direct Observation of the Transition from Indirect to Direct Bandgap in Atomically Thin Epitaxial $MoSe_2$. Nat. Nanotech, (2014); 9 (2), 111–115.
80. Lin, Y.-F., Xu, Y., Wang, S.-T., et al. Ambipolar $MoTe_2$ Transistors and Their Applications in Logic Circuits. Adv. Mat., (2014); 26 (20), 3263–3269.
81.Wilson, J. A., and Yoffe, A. D. The Transition Metal Dichalcogenides Discussion and Interpretation of the Observed Optical, Electrical and Structural Properties. Adv. Phys., (1969); 18 (73), 193–335.
82.Yang, S., Tongay, S., Li, Y., et al. Layer dependent Electrical and Optoelectronic Responses of $ReSe_2$ Nanosheet Transistors. Nanoscale, (2014); 6 (13), 7226–7231.

83. Jo, S.-H., Park, H.-Y., Kang, D.-H., et al. Broad Detection Range Rhenium Diselenide Photodetector Enhanced by (3-Aminopropyl) Triethoxysilane and Triphenylphosphine Treatment. Adv. Mat., (2016); 28 (31), 6711–6718.
84. Ahn, J., Ko, K., Kyhm, J.-h., et al. Near-Infrared Self-Powered Linearly Polarized Photodetection and Digital Incoherent Holography Using $WSe_2/ReSe_2$ van der Waals Heterostructure. ACS Nano, (2021); 15 (11), 17917–17925.
85. Liu, F., Zheng, S., He, X., et al. Highly Sensitive Detection of Polarized Light Using Anisotropic 2D ReS_2. Adv. Funct. Mat., (2016); 26 (8), 1169–1177.
86. Li, J., Han, J., Li, H., et al. Large-area, Flexible Broadband Photodetector Based on WS_2 Nanosheets Films. Mater. Sci. Semicond. Process., (2020); 107, 104804.
87. Pham, P. V., Bodepudi, S. C., Shehzad, K., et al. 2D Heterostructures for Ubiquitous Electronics and Optoelectronics: Principles, Opportunities, and Challenges. Chem. Rev., (2022).
88. Chen, J. J., Wang, Q., Meng, J., et al. Photovoltaic Effect and Evidence of Carrier Multiplication in Graphene Vertical Homojunctions with Asymmetrical Metal Contacts. ACS Nano., (2015); 9 (9), 8851–8858.
89. Mukherjee, S., Maiti, R., Midya, A., et al. Tunable Direct Bandgap Optical Transitions in MoS_2 Nanocrystals for Photonic Devices. Acs Photonics, (2015); 2 (6), 760–768.
90. Zhang, K., Zhang, T., Cheng, G., et al. Interlayer Transition and Infrared Photodetection in Atomically Thin Type-II $MoTe_2/MoS_2$ van der Waals Heterostructures, ACS Nano, (2016); 10 (3), 3852–3858.
91. Radisavljevic, B., Whitwick, M. B., and Kis, A. Integrated Circuits and Logic Operations Based on Single-Layer MoS_2. ACS Nano, (2011); 5 (12), 9934–9938.
92. Elahi, E., Nisar, S., Rabeel, M., et al. Gate-controlled rectification and broadband photodetection in a P–N diode based on TMDC heterostructures. Mater. Adv., (2024); 5(3), 1226–1233.
93. Janardhanam, V., Zummukhozol, M., Jyothi, I., et al. Self-powered MoS_2/n-type GaN heterojunction photodetector with broad spectral response in ultraviolet–visible–near-infrared range. Sensors & Actuators: A. Physical, (2023); 360, 114534.